Water Science & Technology

Water Science & Technology Vol 88 No 11, 2940 doi: 10.2166/wst.2023.386

Inflow and infiltration assessment of a prototype sanitary sewer network in a coastal city in China

Licheng Ye[a], Yu Qian[a,*], David Z. Zhu[a,b] and Biao Huang[a]

[a] School of Civil and Environmental Engineering and Geography Science, Ningbo University, Ningbo 315211, China
[b] Department of Civil and Environmental Engineering, University of Alberta, Edmonton, AB T6G 1H9, Canada
*Corresponding author. E-mail: qianyu@nbu.edu.cn

ABSTRACT

A 16-month monitoring program was conducted on a prototype sanitary system in a coastal city in China. The groundwater infiltration (GWI) on dry weather days and the rain-derived inflow and infiltration (RDII) on wet weather days were quantified and analyzed. The proportion of monthly averaged GWI to total flow can be as high as 70% during the observation period mainly due to the high groundwater level. The results also show that the ratio of RDII volume to total rainfall volume (defined as *R*-value) reaches a limited value of approximately 10% for the studied system when the total rainfall depth increases. A reference indicator R_{lim} for the limited *R*-value was proposed for assessing the conditions of sewer systems in terms of RDII. The R_{lim} value depends on local sewer conditions and in general, a lower R_{lim} value represents a better performance on RDII and vice versa. This study enriches the case studies on the performance of a specific sanitary sewer system on inflow and infiltration in a typical coastal city with exceptionally high groundwater levels, excess rainfall events in the monitoring season and possible typhoon events, which addresses the unique locational and hydrological properties of a representative coastal city.

Key words: asset management, coastal city, inflow and infiltration, sanitary sewer system

HIGHLIGHTS

- The time-period for the 'minimum night flow method' should be adjusted accordingly.
- High infiltration due to high groundwater levels was observed specifically for the study site.
- The ratio of RDII volume to total rainfall volume (*R*-value) tends to be limited as rainfall increases for all RDII events.
- The limited *R*-value for high rainfall events was proposed for assessing the performance of sewer systems.

GRAPHICAL ABSTRACT

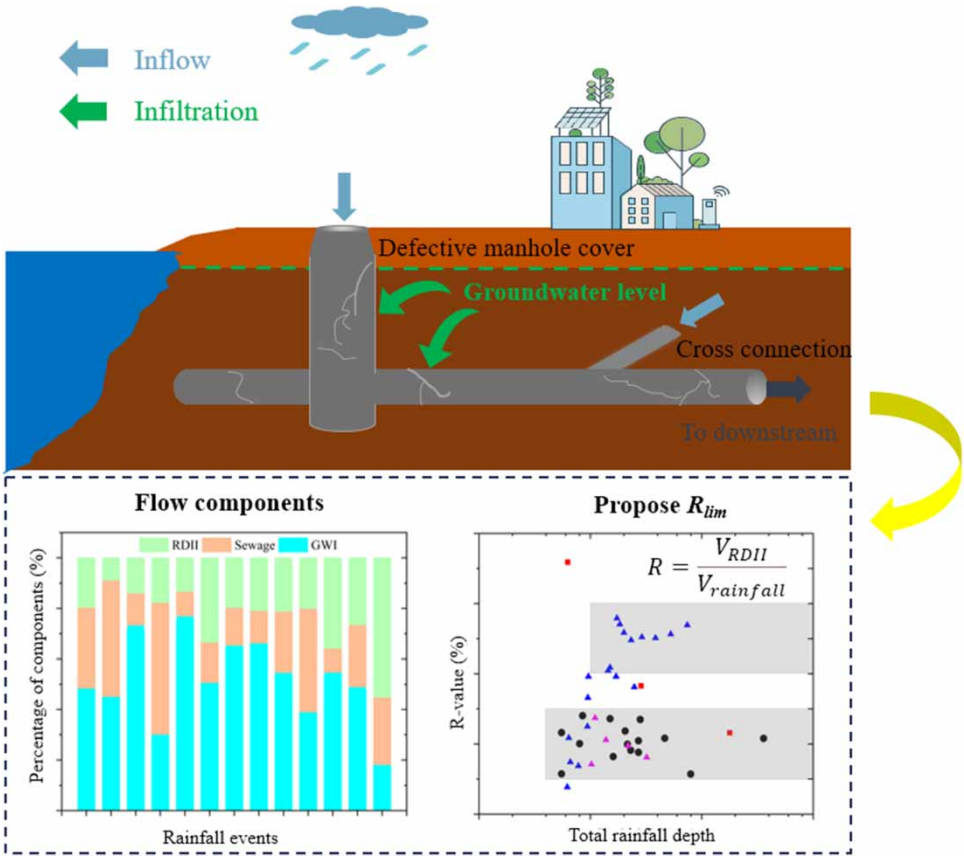

1. INTRODUCTION

Urbanization has resulted in the rapid development of urban drainage systems in cities around the world. The total length of urban drainage systems including sanitary, storm, and combined systems in China has almost doubled in the last decade from 439,000 km in 2012 to 803,000 km in 2020 (National Bureau of Statistics of China 2022). Due to ageing systems, defects in sewers, illicit connection and other factors, extraneous water enters the sewer systems causing sewer inflow and infiltration (I/I) which mainly consists of groundwater infiltration (GWI) and rain-derived inflow and infiltration (RDII). The RDII is generally composed of rainfall-derived inflow (RDI) and rainfall-induced infiltration (RII), where RII is also called delayed infiltration in terms of the flow response time of stormwater infiltration which is between the rapid response of stormwater direct inflow and the slow response of GWI (Sowby & Jones 2022).

The extraneous water increases hydraulic loadings of sanitary sewers and wastewater treatment plants (WWTPs). In extreme cases, the I/I volumes can even be higher than the wastewater volume (Bertrand-Krajewski *et al.* 2006), which affects the pollutant removal efficiency of WWTP and results in additional costs in processing the wastewater (Ellis &Bertrand-Krajewski 2010; Dirckx *et al.* 2016; Jenssen Sola *et al.* 2018). In China, the inflow and infiltration generally dilute the sewage and cause low chemical oxygen demand (COD), which may cause issues in the WWTP. Inflow and infiltration can also cause the volume of water in the sanitary network to exceed the maximum operating capacity and cause sanitary sewer overflows (SSOs) incidents, especially during rainfall events (Crawford *et al.* 1999; USEPA 2007). Furthermore, the GWI can flush the surrounding soil into the sewer system, accelerating the structural deterioration, and causing sinkholes or surface settlements due to soil erosion around the defective sewers (Kracht *et al.* 2008; Guo *et al.* 2013). The studies above illustrate that the negative impacts of I/I on the urban environment and municipal infrastructure can be significant. The I/I level can be used as an indicator to characterize the integrity of the pipe network (Zhang *et al.* 2018). However,

due to the influence of many factors such as the drainage regulations, physical conditions of the pipes and rainfall patterns, it is generally difficult to quantify the amount of extraneous water (Karpf & Krebs 2011).

Using qualitative methods to roughly evaluate the sanitary system is an effective strategy to reduce the amount of workload and costs (Thapa *et al.* 2019). Generally, physical methods (e.g. visual and odor inspection, dye testing or smoke testing, closed circuit television (CCTV) inspection and temperature sensing) are used to qualitatively analyze the inflow and infiltration in sewer systems (Hoes *et al.* 2009; Irvine *et al.* 2011). Shehab & Moselhi (2005) developed an automated system based on pattern recognition, image analysis and artificial intelligence techniques to automatically detect and classify infiltration of sewer pipes. An increasing number of artificial intelligence (AI) technologies have also been developed to analyze CCTV images for characterizing sewer defects in recent years (Cheng & Wang 2018; Zhou *et al.* 2022; Sun *et al.* 2023). Tracer methods (e.g., chemical tracer, biological markers, and stable isotope) based on material balance have been proven to be accurate in quantifying I/I (for example in Mattsson *et al.* 2016; de Ville *et al.* 2017; De Bondt *et al.* 2018; Zhao *et al.* 2020). Kracht & Gujer (2005) and Kracht *et al.* (2007) successfully applied COD and stable isotope as tracers to quantify infiltration in the sewer systems in Europe, respectively. Zhang *et al.* (2017) applied four tracers for accessing RDII and concluded that conductivity has the best reliability and sensitivity for RDII simulation compared with the other three tracers including COD, NH_4^+-N, PO_4^{3-}-P. The key to this type of method is to find a reliable tracer or combination of tracers in local wastewater or extraneous water.

With respect to quantitatively analyzing methods on I/I, Weiß *et al.* (2002) proposed the 'triangle' method and 'moving-minimum' method in the study of 34 combined sewage systems in Germany. The 'triangle' method assumes that the domestic sewage flow is constant in a certain period. Therefore, this method can only obtain the average I/I, and the variation of the infiltration process over time is not shown by this method. The 'moving-minimum' method assumes that the sum of the sanitary sewage plus I/I on any day is equal to the minimum daily flow in the 21 days before the day of concern, but this method lacks physical background. Due to the diurnal pattern of domestic water use, the minimum effluent flow generally occurs at night, and the 'minimum night flow method' was applied for quantifying I/I based on the flow-based method (Ellis & Bertrand-Krajewski 2010). It is based on the assumption that the GWI rate is roughly close to the minimum night flow (Kracht *et al.* 2008). De Bénédittis & Bertrand-Krajewski (2005) studied the uncertainty of infiltration estimation using the 'minimum night flow method' and found that a sufficient duration of dry weather days was needed to ensure the accuracy of this method. A sufficient observation time can reduce the uncertainty to about 10% as indicated in De Bénédittis & Bertrand-Krajewski (2005). A number of hydraulic model-based methods have also been proposed for I/I analysis (Li *et al.* 2008; Karpf & Krebs 2011). Liu *et al.* (2021) proposed a statistical model based on logistic regression to predict the probability of GWI. Machine learning was used to calibrate, validate, and test the model. Model influence parameters were determined as pipe material, size and shape, soil condition, and groundwater level.

With respect to field monitoring studies, Zhang *et al.* (2018) estimated the inflow and infiltration for three rainfall events in a separate sanitary sewer system. Chen *et al.* (2022) conducted a similar monitoring campaign to studying the inflow and infiltration in an aged residential compound in China, which was retrofitted from a combined to a separate system during the monitoring period. It was found that the inflow and infiltration characteristics are different in different types of drainage systems. Water balance methods or flow-based methods are suitable for closed systems. However, when there are overflows, this method will produce errors, because the method does not take into consideration the water exiting the system (Jenssen Sola *et al.* 2018). For more complex pipe connections, the installation location of the monitoring equipment can be determined after simulation with software such as storm water management model (SWMM). In the study of Chen *et al.* (2022), the placement of the water level meters was determined based on SWMM simulation. Moreover, the local error of the I/I assessment method needs to be considered for field studies. For example, for the tracer method, it is necessary to investigate the maximum residence time in the pipeline and the potential deposition of markers used in the catchment area of the study area (Xu *et al.* 2016; Yang *et al.* 2021).

The above studies mainly focused on general understandings of I/I in inland cities. For coastal cities, the performance of the sewer systems may be different due to the high groundwater level, excess rainfall, possible typhoon events and hence assessing the I/I under extreme conditions is necessary. The study area is a coastal city, Ningbo, Zhejiang province, in east China which experiences abundant total annual precipitation (average of the multi-year total annual precipitation 1,525 mm), with large seasonal differences in rainfall, susceptible to short-term heavy rainfall in summer and autumn under the influence of typhoons, and 60% of the total annual precipitation in the main flood season from May to September (Ningbo Meteorological Service Center (accessed 30 March 2023)). The general impact of groundwater or specific rainfall

events on a prototype sanitary system is therefore to be assessed. The present study mainly focuses on the relationship and pattern of the response of hydraulic operating parameters, such as flow and water depth in a prototype sanitary sewer system, to external conditions, such as rainfall and groundwater level. The goal is to find a method to assess the performance of inflow and infiltration of a prototype sanitary sewer network in a coastal city. This study enriches the case studies on the performance of sanitary sewer systems on inflow and infiltration and may provide key references for inflow and infiltration management in coastal regions.

2. MATERIALS AND METHODS

2.1. Site description

This study was conducted in a residential area in Ningbo, Zhejiang, China, as shown in Figure 1. The drainage system in the study area is relatively isolated with a service area of 0.32 km^2. The sanitary sewer system in the study area collects sewage from three residential compounds and the discharge path is generally clear with no industrial wastewater discharge in this area. The sewers are PVC pipes with a diameter of 300 and 400 mm and the total length of the pipes is about 2 km. The pipes are full pipe flow during the period of our monitoring work given the high groundwater level. This area was chosen for the I/I field study mainly because the sewer networks are subject to high groundwater levels, which might be a potential risk of inflow and infiltration. The monitoring location WF1 is located at the downstream pipe of the sewer network in the study area, where all sewage in the study area is collected at WF1 and eventually flows into the trunk.

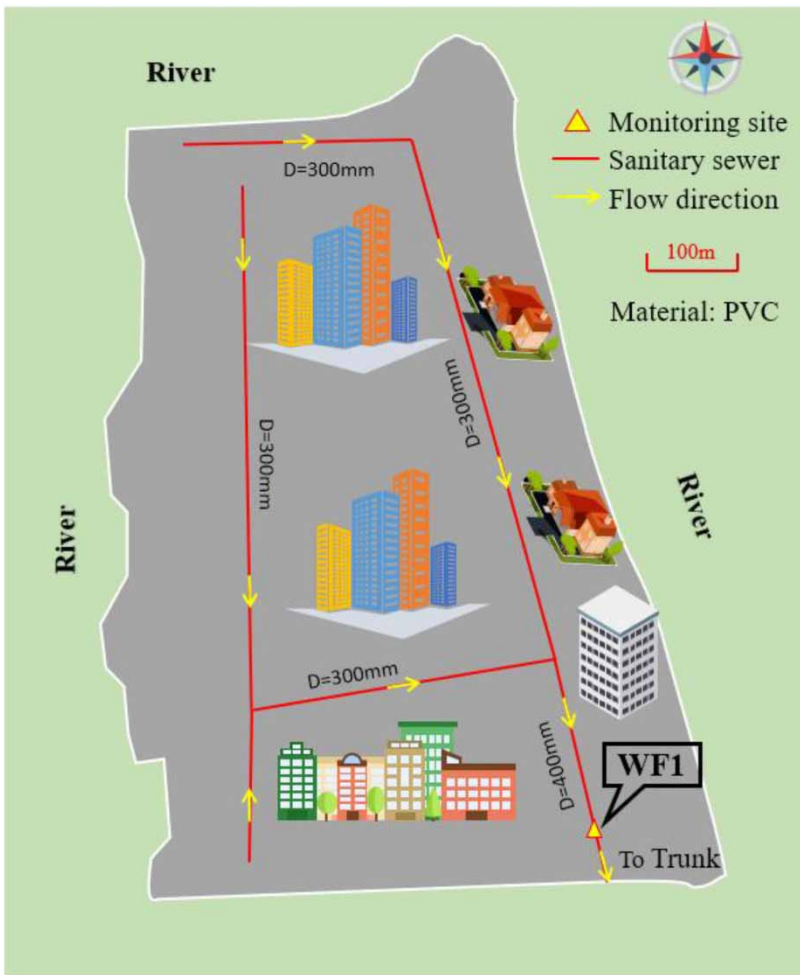

Figure 1 | Schematic of the study area and the sewer connections.

2.2. Data acquisition and preparation

An online flowmeter THWater Smart Drainage Monitoring Flowmeter (THWater Official Site (accessed 16 June 2023)) was installed at the monitoring location WF1. The flow meter was able to measure both flow rate and velocity as well as water depth. It has a velocity measurement resolution of 0.001 m/s, an accuracy of 0.03 m/s, range of $\pm$ 6 m/s. The flow meter was well maintained and pre-calibrated with a HACH FL900AV Flow Meter (HACH Official Site (accessed 16 June 2023)) before installation. This type of flow meter also measures water depth at a resolution of 0.001 m and a range of 10 m. The sampling frequency for the monitoring program was one sample per minute for both velocity, flow rate and water depth. Precipitation and groundwater data were collected from the local hydrology department with a measurement resolution of 0.5 mm at 5 min and 0.01 m at 1-day intervals, respectively. The invert elevation of WF1 was 2.348 m below sea level.

The WF1 was continuously monitored from August 23, 2021, to December 31, 2022, and a total number of 659,590 sets of 1-min raw data was collected during the monitoring period. To improve the accuracy of data and eliminate errors, the raw data were pre-processed before analysis to exclude defective data where the velocity was less than 0.03 m/s due to the value falling below the accuracy of the equipment. The data then were summed up for hourly flow and daily flow. An example of data treatment is shown in Figure 2 from November 10, 2021 to November 24, 2021. The magenta line represents the 1-min raw data, and the black and blue lines show the daily and hourly averaged flow respectively. As shown in Figure 2, the rainfall-induced flow response in hourly time series shows the RDII pattern well, and therefore in the following RDII analysis, flow is on an hourly time scale.

The dates for dry weather flow were selected based on the rules of Karpf & Krebs (2011) and Staufer *et al.* (2012) where the dry weather days are defined as the rainfall intensity under 0.3 mm/day for the day and the day before in order to exclude the contribution of stormwater runoff to the measured flow rate. A total number of 105 dry weather days was selected. A wet weather day was defined as a period containing a rainfall event with more than 2 mm of precipitation in a 6-h period (Rezaee & Tabesh 2022). A total number of 15 rainfall events were identified for the analysis of RDII, one of which was affected by a typhoon event.

3. RESULTS AND DISCUSSIONS

3.1. Dry weather flow and GWI

The difference in water consumption habits between weekdays and weekends may result in variations in the total volume of flow in the network. Therefore, the 105 selected dry weather days were divided into 69 weekdays and 36 weekends. The daily sewage flows of the two categories were calculated. The flow at the monitoring point was summed to obtain the daily flow as

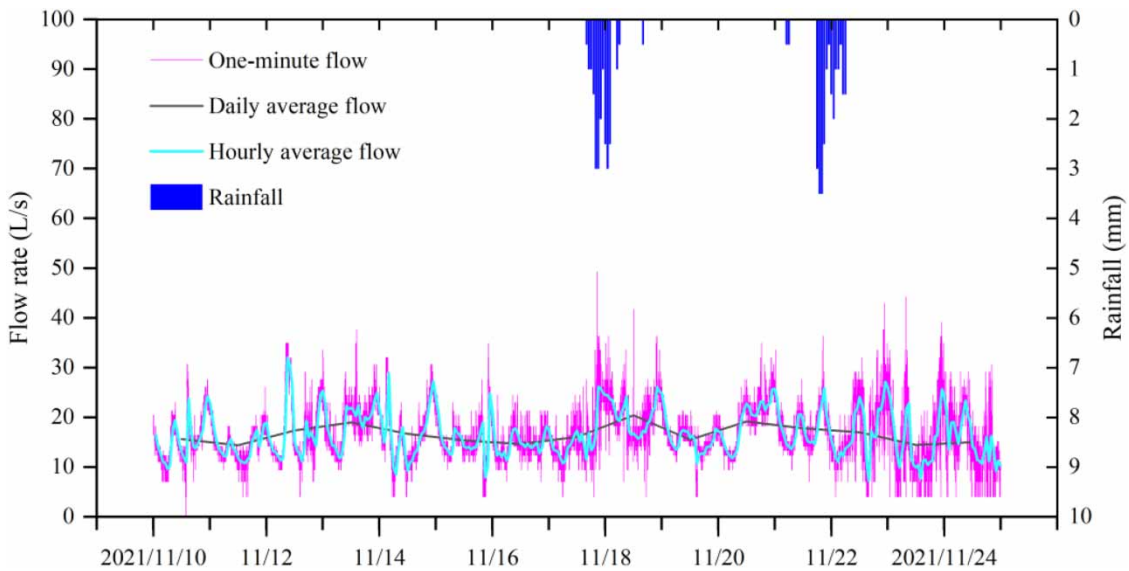

Figure 2 | Example time series of 1-min flow (raw data), daily flow, and hourly flow (both processed data).

shown in Figure 3. The time represented by the abscissa in Figure 3 is not continuous due to the interruption of rainfall events. As can be seen from Figure 3, the mean value of weekend flow on dry days is 1,508 m^3/d, which is about 7% higher than the weekdays at 1,404 m^3/d. The main reason for the flow difference between weekdays and weekends is the residents' living patterns. Given the high proportion of weekdays at 65% of total analyzed days and only 7% in total flow difference between weekdays and weekends, the next session discussed the analysis of the diurnal flow variation over the 69 dry weather weekdays.

The diurnal flow variation was first analyzed. The raw data were moving averaged in a 15-min window for a manageable data amount as well as flow details plotted in Figure 4. A box plot was drawn and outliers were further excluded, with outliers defined as less than Q1 − 1.5*IQR or greater than Q3 + 1.5*IQR (IQR, interquartile range; Q1, first quartile; Q3, third quartile). There are two peaks daily, one in the morning and one in the evening mainly due to high water consumption by residents shown in Figure 4. During the period from 7:00 to 10:00, the flow showed an obvious rapid rise, from about 13 L/s to a maximum of about 19 L/s in 3 h due to the morning water consumption peak. There was a slight increase at 12:00, lasting for about 1 h, which corresponds to lunchtime. Between 14:00 and 16:00 was stable and there was a slight increase after 16:00. The evening peak is from about 19:00 to 1:00 the next day, with a slow increase in flow, reaching a mean maximum of about 22 L/s at about 23:00 for bedtime.

At the study site, the flow rate showed a downward trend from 2:00–4:00. In the literature, the time-period used for the 'minimum night flow method' for GWI analysis was 2:00–4:00 or 0:00–6:00 in Ellis & Bertrand-Krajewski (2010) and Chen *et al.* (2022) respectively. In this study, it was found that the lowest flow rate in individual days occurred between 4:00 and 6:00. Although 6:00 shows the lowest average flow rate, it is still believed that the period of 4:00–6:00 should be used for a more general coverage of days of the lowest flow rate in a day. It was proposed in this study that the time-period for this specific location for the 'minimum night flow method' should be adjusted to 4:00–6:00 for GWI analysis. In general, the proper time-period of application of this method should be adjusted by local actual field monitoring. This could be explained by the different local properties of groundwater level, pipe condition, residents' water usage pattern, and the size of the sewer system.

Figure 5 shows the results of the monthly variation of GWI using the 'minimum night flow method' for the study area. Months with less than 8 dry weather days were excluded to reduce uncertainty. The average ground elevation was

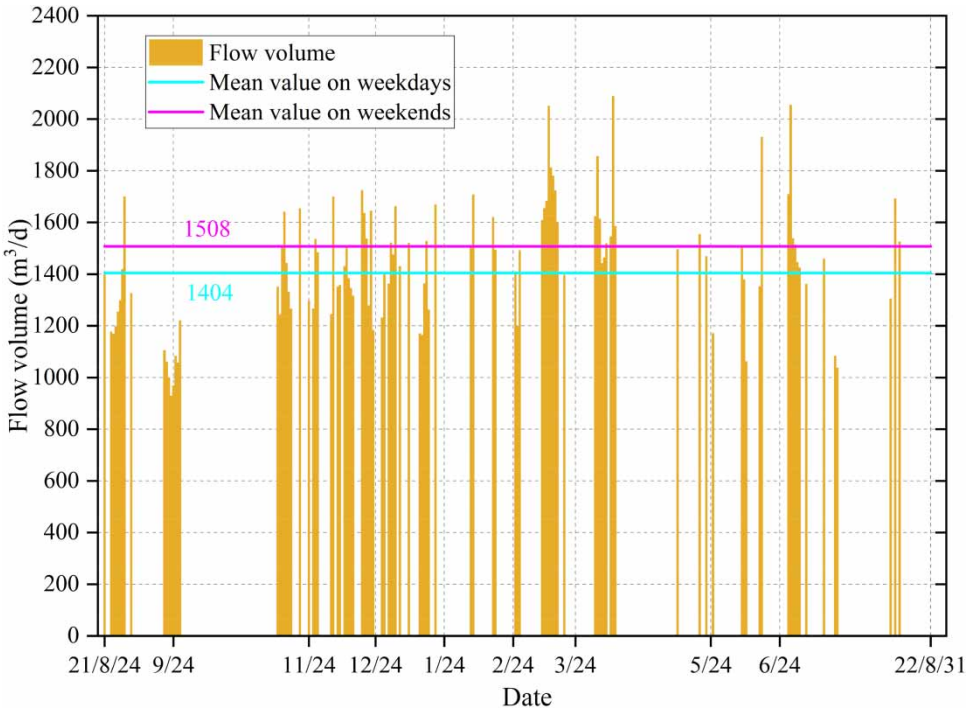

Figure 3 | Daily change of flow volume on dry weather days.

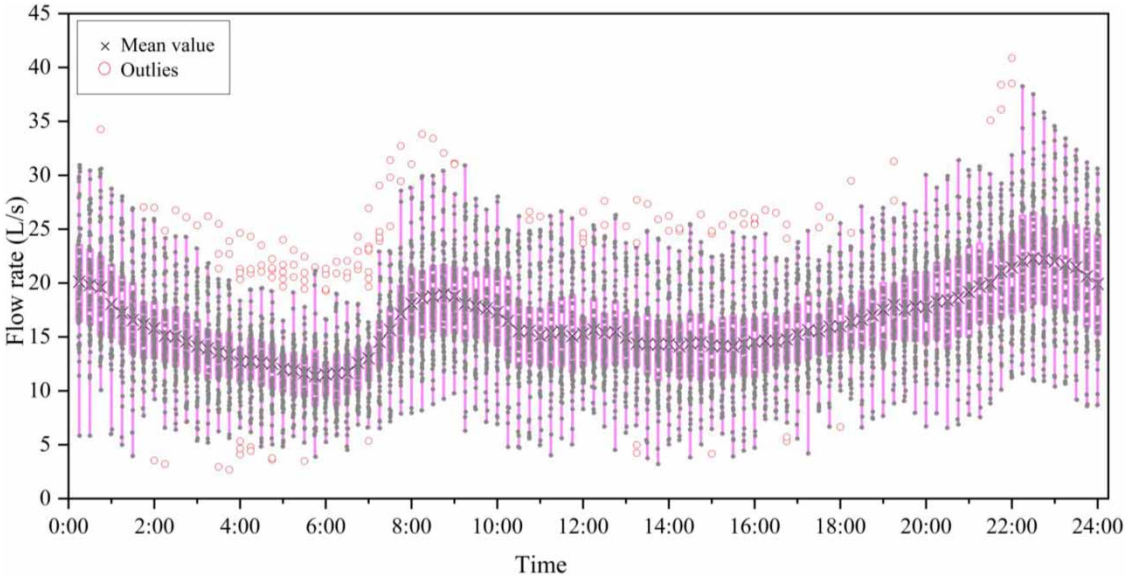

Figure 4 | Plot of selected 69-day data for dry weather flow variation.

2.968 m while the monthly average groundwater elevation remained at 1.91 m with slight variation, which was 4.2 m above the invert elevation of the sanitary network at −2.348 m. According to Figure 5, the minimum value of the average GWI rate at 9.1 L/s occurred in September 2021, and the values in other analyzed months were about in the range of 12 ± 0.6 L/s. The percentage of daily infiltration amount was found to be about 75% of the total flow in November 2021, which was relatively high compared with 18% of a combined sewer system in Ningbo before upgrade average sewage flow at 11.4 ± 1.3 L/s, and GWI at 2.1 ± 0.4 L/s (Chen *et al.* 2022) and average 35% for the 34 sewage systems investigated in Germany (Weiß *et al.* 2002).

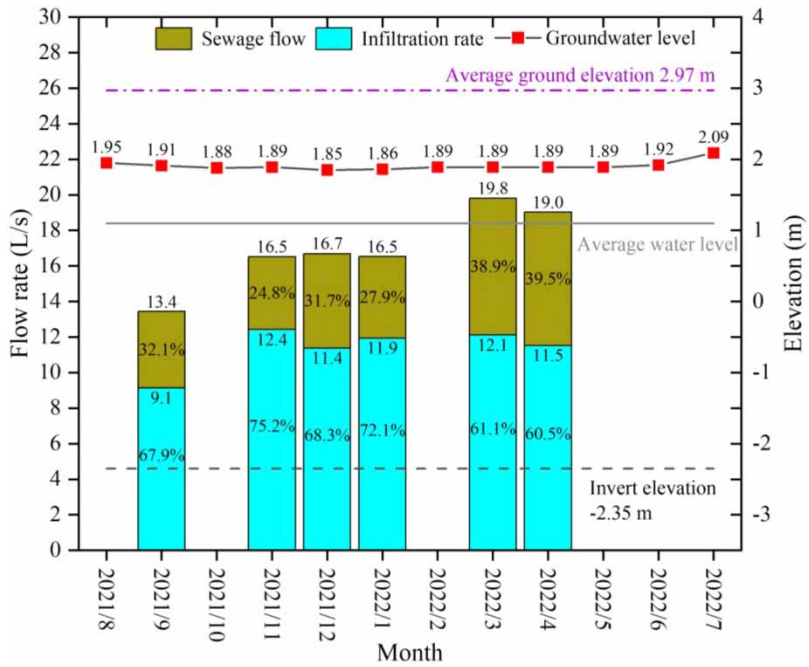

Figure 5 | The monthly change of GWI.

The typical value of average daily water usage in megacities of China is 210–340 L per capita per day (LPCD) according to regional design guidelines (Ministry of Housing & Urban-Rural Development of the People's Republic of China 2018). Assuming the GWI accounts for 70% of the total flow, the service area corresponds to a population of approximately 1,200–2,000, which is roughly in accordance with the occupancy of the built dwellings in this area. Two time series, November 10 to 28, 2021 and December 4, 2021 to January 8, 2022, were selected for cross-correlation analysis between daily GWI rate and daily groundwater level. The cross-correlation analysis did not yield valid results for both time series data mainly due to the less variation of groundwater level and GWI value on a daily scale. The GWI usually depends on factors such as groundwater level, soil characteristics and sewer conditions (Karpf & Krebs 2011; Thapa *et al.* 2019; Liu *et al.* 2021). The effect of high groundwater levels on the GWI is a very important influencing factor in this study area. The sanitary sewer system operates at a high groundwater level, resulting in a high infiltration due to seepage phenomena, as the water level in the network is well below the groundwater level. Groundwater level and infiltration rate generally do not fluctuate over time in this sewer network, and the influence of their variations could not be observed. Theoretically, under certain physical conditions of the network, the infiltration into the sewer network and the difference between the water level of the pipes and the groundwater level should satisfy a certain relationship such as Darcy's law and be positively correlated. But in the present sewer network it is not possible to observe it due to less variation.

There are two other reasons for the high percentage of infiltration. First, the 'minimum night flow method' calculates the infiltration volume based on the infiltration rate as a constant value, but the infiltration rate actually varies over time, which causes errors. In a previous study, the infiltration volume of a month obtained based on this method was 71 and 93% higher than the results of the 'triangle' method and 'moving-minimum' method on their studied catchment (De Bénédittis & Bertrand-Krajewski 2005). Second, most of the residential buildings in the study area are newly built or under construction, the total daily sewage discharge is relatively low due to few permanent residents, and the denominator is small when calculating the infiltration percentage.

3.2. Quantification of RDII in selected rainfall events

Representative rainfall events were selected to estimate the impact of RDII of the studied system during the monitoring period at the monitoring site WF1. The raw flow data obtained per minute was hourly accumulated. As dry weather flow was relatively stable, selecting two dry days' flow in the vicinity of a rainfall event can effectively represent the base flow at the time of the rainfall event, and hence the flow in the system two dry days before or after the rainfall events was selected as the reference flow. In this study, the time-period of RDII is defined as: from the beginning of the rainfall with instantaneous intensity higher than 0.5 mm/h to the time when the flow in the system decreases and reaches 97% of the reference flow and lasts for 2 consecutive hours. The time-period of flow increase during a rainfall event was defined as the rainfall event dominant period, while the period dominated by infiltration was defined as the time-period after the main rainfall period of rainfall events until the whole RDII process ends. Meanwhile, the real-time water depth was compared with the corresponding water depth in reference dry weather days (reference water depth) for auxiliary assessment.

The RDII-influenced wet weather day flow volume $V_{\mathrm{wet,i}}$ minus the reference dry day flow volume $V_{\mathrm{dry,i}}$ for the same period is defined as the RDII value V_{RDII}. The proportion of RDII to rainfall volume is defined as R and it can be calculated by Equation (1). V_{rainfall} was calculated by multiplying rainfall depth by catchment area.

$$R = \frac{V_{\mathrm{RDII}}}{V_{\mathrm{rainfall}}} \tag{1}$$

Figure 6 shows the RDII process of four representative rainfall events. Points A, B, C, and D stand for the start of the flow response, the maximum flow increase rate, the end of the main rainfall period of the rainfall event and the end of the RDII process, respectively. In Figure 6(a), the rainfall started at 15:00 on November 17, 2021 and ended at 16:00 on the second day, with a total rainfall duration of 14 h and total precipitation of 23 mm. The maximum intensity of 3 mm/h occurred 4 h after the start of the event, and the total rainfall volume was 7,360 m^3. The flow rate in the system exceeded the dry weather reference flow rate at about 1 h after the start of the rainfall event at point A in Figure 6(a). The maximum flow increase rate was at point B, where the flow rate increased from 16 L/s in the preceding hour to over 25 L/s at this point. The main rainfall period of the rainfall event ended at point C, from which point the influence of infiltration gradually became dominant. The total RDII volume was 671 m^3 as shown in the shaded area in Figure 6(a), and the R-value was 9.1%. The different shapes of

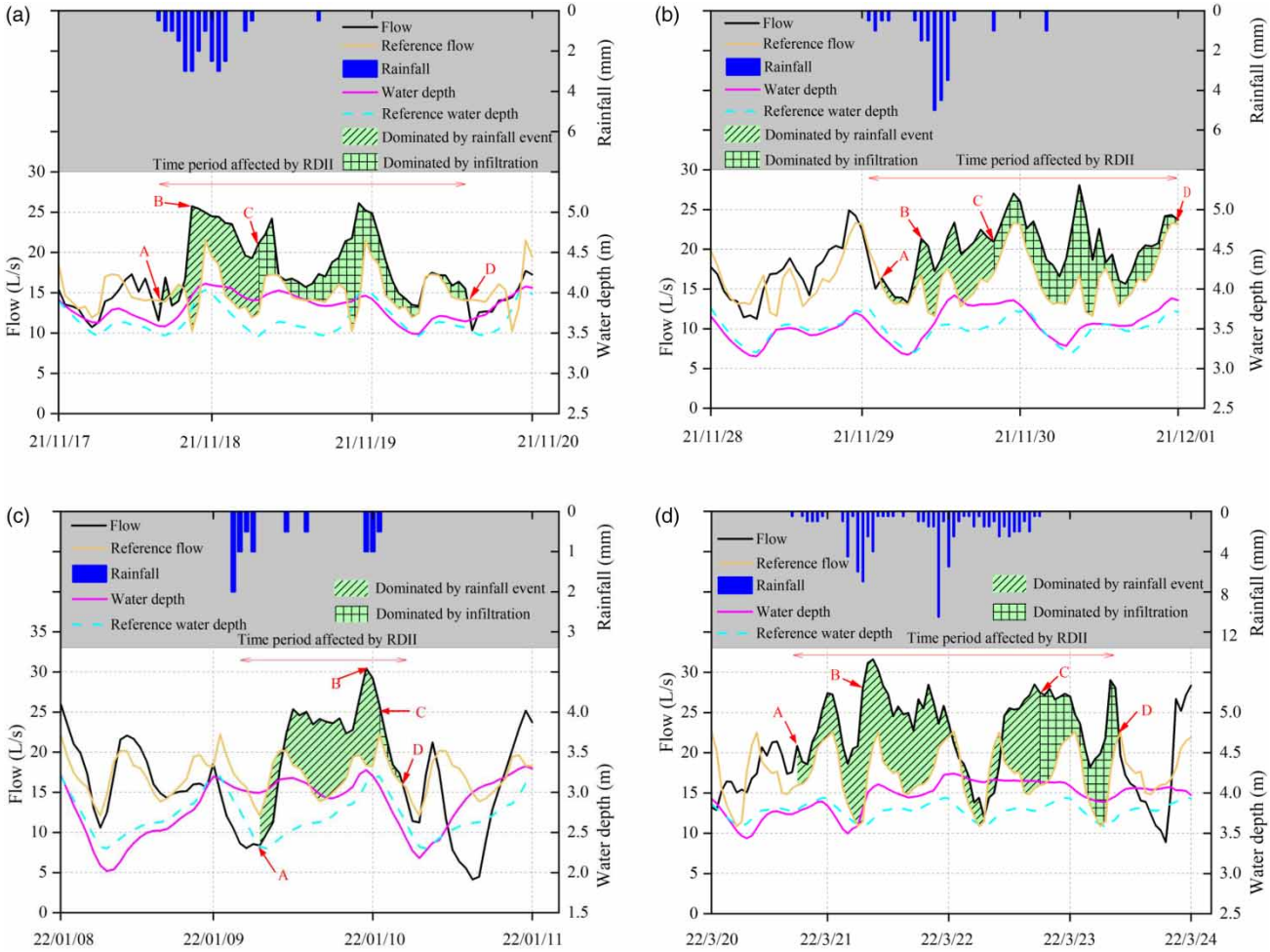

Figure 6 | Representative RDII response processes for four rainfall events. *Note:* reference flow and reference water depth are from dry days' averages in the vicinity of rainfall events.

the shaded areas in the figure represent periods when the flow increase was dominated by rainfall events and infiltration, respectively. The RDII process lasted for about 47 h and ended at point D which showed that the RDII events affected the flow for 22 h after the rainfall events. The water depth was slightly above the reference water depth at the start of the rainfall, and the difference between the two increased when the rainfall intensity reached 3 mm/h and the cumulative rainfall depth of 4 mm.

In Figure 6(b), the total rainfall depth was 21.5 mm, and the rainfall started at 0:00 on November 29, 2021 and ended at 4:00 on the second day with a total duration of 13 h and a maximum rain intensity of 5 mm/h at 10 h after the start of the event. The total rainfall volume was 6,880 m^3. The flow rate exceeded the dry weather reference flow rate about 2 h after the start of the rainfall at point A in Figure 6(b). The maximum flow increase rate was at point B and the flow rate was 21 L/s to a peak. The RDII process lasted for about 48 h to end at point D and the total RDII volume was 686 m^3. The *R*-value was calculated to be approximately 10.0%. The flow increase dominated by rainfall events obviously lasted approximately 18 h and dominated by infiltration for about 28 h after the main rainfall period of the rainfall event (at point C). The water depth response was observed when the rain intensity reached 1.5 mm/h (cumulative rainfall depth reached 3 mm) and the water depth was higher than the reference, and it was maintained for only 16 h.

It should be noted that specifically in Figure 6(c) and 6(d), it was not straightforward to determine the onset of flow response by observing the change in absolute values, so the gradient of the flow curve for the RDII process and the corresponding referenced dry weather flow curve were calculated and the difference in the trend of the curve change was used

as an indicator of the initiation of the RDII response. In Figure 6(c), the rainfall event started at 2:00 on January 9, 2022 and ended at 1:00 on the second day for 9 h with a total rainfall depth of 8 mm (volume of 2,560 m^3). Calculation of the slope of the flow curve showed that the flow in the sewer began to show an obvious steep upward trend 4 h after the start of the rainfall at point A in Figure 6(c). The flow continued to increase reaching a maximum value of about 30 L/s at point B after 17 h, after which the flow began to decrease and entered a period dominated by infiltration after the end of the rainfall (at point C). In this case, the time-period of flow increase dominated by rainfall events occupied the vast majority of the time-period of the RDII process due to the relatively small rainfall totals and low rainfall intensity except for the first hour of the rainfall event. The RDII process lasted for approximately 26 h to end at point D and the RDII volume was 257 m^3. The *R*-value was approximately 10.1%. The rainfall event started with a rain intensity of 2 mm/h, and the water depth soon responded significantly and lasted for 22 h.

In Figure 6(d), the total rainfall depth was 79.5 mm, the rainfall started at 17:00 on March 20, 2022 and ended at 18:00 on March 22, 2022, with a rainfall duration of 43 h and a maximum rain intensity of 7 mm/h at 14 h after the start of the event. The total rainfall volume was 25,440 m^3. The flow rate was already slightly greater than the dry weather reference flow rate before the rainfall started. After calculating the slope of the flow curve, it was found that the flow response started to appear 1 h after the start of rainfall at point A in Figure 6(d). The RDII process ended at point D and the RDII volume was 1,455 m^3. The *R*-value was calculated to be approximately 5.7%. There were multiple flow peaks during the RDII process, with the maximum flow increase rate at point B. In this case, the rainfall event was of long duration and high intensity. The period of flow increase dominated by rainfall event obviously lasted approximately 49 h and dominated by infiltration for about 15 h after the rainfall event (at point C), which was related to characteristics of rainfall events. The water depth was a visible rise when the rain intensity reached 7 mm/h (cumulative rainfall depth 16.5 mm), and this high water depth remained for period of time until after the flow had already returned.

The initial water depth response for the above four rainfall events occurred when the instantaneous rainfall intensity reached 3, 1.5, 2, and 7 mm/h, and the corresponding cumulative rainfall depth was 4, 3, 2, 16.5 mm, respectively. The duration of high water depth receding at the end of rainfall is related to the duration of high-intensity rainfall during the rainfall process and increases with the latter. At this stage, the water content of the soil was high due to the high groundwater level in the study area. With relatively low permeability, the surface runoff generates relatively quickly causing more water to enter the system via surface openings such as manhole covers. The relatively small diameter of the storm sewer ranging from 500 to 700 mm in the separate drainage system leads to insufficient drainage capacity. The longer the duration of high rainfall intensity, the more the surface water accumulates, which cannot be drained by storm systems efficiently. Due to the limited capacity of sanitary sewers, the rapid flow increase caused by rainfall events with high intensity resulted in a significant volume increase in the sewer system. The rainfall-derived flow in the studied system did not always coincide with the water depth variation in the manhole given the full pipe flow condition in this study due to the unique properties of the coastal city on groundwater level, and precipitation patterns.

In this study, for the majority of rainfall events, the time lag between the initial flow response of the sanitary sewer system and the rainfall was 1–2 h. Chen *et al.* (2022) found the time of response generally within the range of 30–40 min in the RDII study of a combined sewer system in Ningbo, and this difference is mainly due to the different types of drainage systems, service area of the systems and runoff coefficient. Although the catchment area of the study area is relatively small, the service area of Chen *et al.* (2022) was only about a quarter of this study. This could be one reason why the initial flow response was faster. Based on the physical background, the component of increased flow during a rainfall event is mainly rain-derived inflow (RDI), and after a rainfall event is rainfall-derived infiltration (RII). The total rainfall depths for the rainfall events in Figure 6(a) and 6(b) were approximately the same, but there are significant differences in the characteristics of rainfall. The *R*-values calculated are similar for these two events. For a long-duration but low-intensity rainfall event, the *R*-value will be slightly lower. The contribution of RDII to the total flow was 21, 20, 14, and 26% and the calculated *R*-value was 9.1, 10.0, 10.1, and 5.7% respectively for the examples in Figure 6(a)–6(d).

The percentage of GWI, sewer flow and RDII to the total flow for the 13 selected rainfall events are shown in Figure 7. Event 13 was a typhoon event, and as can be seen from Figure 7, the total rainfall reached 358.5 mm and the percentage of RDII reached 55%, which was much larger than the other two components. The percentage of RDII for events with large total rainfall (Event 11, Event 12, and Event 13 all exceeding 40 mm) was generally greater than the percentage of RDII for events with small total rainfall. For events with total rainfall less than 20 mm (Events 1–5), the percentage of RDII did not exceed 20%. The percentage of RDII was lower than that of GWI for all events except Event 13. The percentage

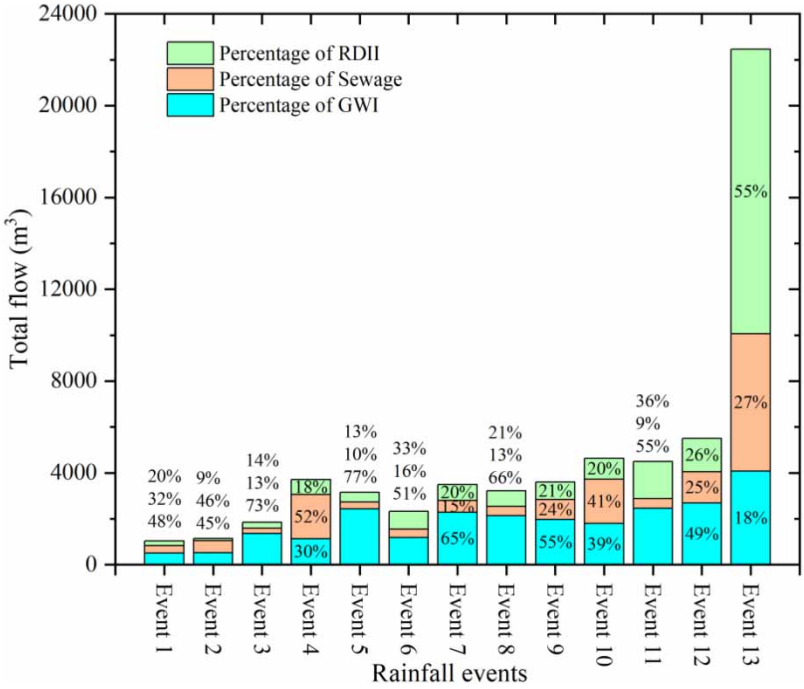

Figure 7 | Percentage of components in representative rainfall events.

of extraneous water (GWI plus RDII) to the total flow is relatively high, and a total of 11 events exceed 65%. The infiltration contributed to the majority of the total flow, for this separate system, the proportion of extraneous water entering the system through the inflow (RDI) path is limited and the main source is infiltration from groundwater and rain-induced sources.

Figure 8(a) and 8(b) shows the relationship between RDII volume and total rainfall volume, *R*-values and total rainfall depth, respectively, for the 15 rainfall events during the monitoring period. The results of this study were compared with Zhang *et al.* (2018) and Chen *et al.* (2022). The systems in this study and Zhang *et al.* (2018) are both separate sanitary sewer systems. Chen *et al.* (2022) assessed the performance of the drainage system and quantified the RDII before and after the upgrade where a combined sewer system was retrofitted to a separate one in an old residential area in Ningbo, China. As seen in Figure 8(a), the RDII volume of these studies show the same trend where the value increased with increasing rainfall volume. For this study, the RDII volume increased from 101 to 12,391 m^3 with a rise in precipitation from 5.5 to 358.5 mm. The slope of the separate drainage system is smaller than that of a combined one, which could explain why the percentage of rainfall converted to RDII was lower in a separate system due to the limited path where the extraneous water can enter the system.

For Figure 8(b), the *R*-value curve in this study stays at a relatively stable value at about 10% (±5%) for the study area, while the results of Chen *et al.* (2022) before system upgrade increased with the total rainfall and reached about 25% (±5%). For the separate system in the present study, the defects of sewers have a maximum capacity for extraneous water to enter, but this capacity is relatively small. Although the amount of RDII increases with the total rainfall, the percentage of volume that enters the sanitary sewer system is limited to about 10% of the total rainfall volume for the studied system regardless of the rainfall intensity. The fluctuations of *R*-values may be related to factors such as rainfall patterns and subsurface conditions. For the result of Chen *et al.* (2022) after the system upgrade, the *R*-values reduced to a lower range at about 10% (±5%). For Zhang *et al.* (2018), the *R*-value curve shows a decreasing trend with the increasing total rainfall. This means that the system is probably in a better condition with a lower *R*-value when the rainfall increase. The curve of the separate system in Zhang *et al.* (2018) shows a downward trend which is contrary to the combined system in Chen *et al.* (2022) (before the upgrade) and the present study. According to Zhang *et al.* (2018), although the total volume of RDII increases with the rainfall volume (Figure 8(a)), the ratio of the volume of rainfall entering the sewer system to the total rainfall volume decreases with the rainfall volume.

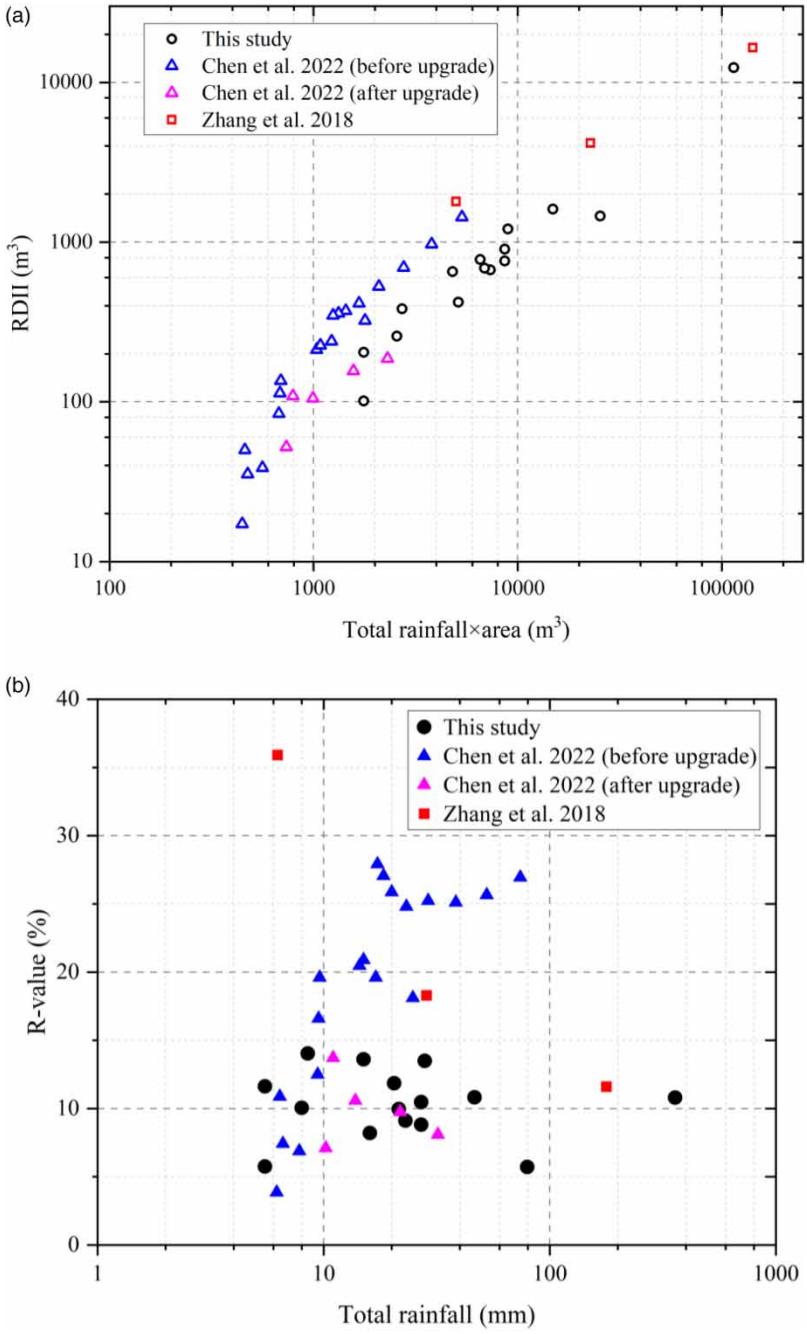

Figure 8 | The relationship between RDII and rainfall.

Although only one monitoring point was used in this study, the upstream of this sanitary sewer system has good independence and all the flow from the upstream passes through this monitoring point. For larger sanitary networks, selecting monitoring points according to the catchment area will provide more desirable effects. For this study, the analysis is only for a specific sanitary sewer system. For other systems, the performance will be different, but the general trend should be similar. The capacity for extraneous water in a sewer system is limited. When the rainfall exceeds a certain level, it will reach a limited situation which can be defined as R_{lim} in this study. For the current system, the limited capacity R_{lim} is 10% ($\pm$5%). This capacity mainly depends on the maximum hydraulic capacity of the system itself, the distribution of the number and location of defects and the percentage of RDII entering the system by different paths.

Similarly, the value of R_{lim} is about 25% in the combined system in Chen *et al.* (2022) before the upgrade and about 10% after the upgrade. The different R_{lim} values may be the results of the type and physical condition of specific systems, differences in the path of extraneous water entering the system and the ageing of the systems. For a specific sewer system, if the R_{lim} is rising, it means that the condition of the system is deteriorating and vice versa. The RDII into the local separate sewer system may be in a similar situation, the R_{lim} values of this study and Chen *et al.* (2022) after upgrade are both approximately 10%, which requires further exploration such as a quantitative comparison of the physical conditions between the two systems. For the above discussion, a reference indicator R_{lim} can be proposed to assess the conditions of sewer systems in terms of RDII. In addition, in the study of Chen *et al.* (2022), the results of inflow and infiltration can be measured in rainfall events with rainfall amounts above 5 mm due to surface ponding, and interception by flat roots and vegetation. In this study, rainfall events less than 5 mm during the observation period were also observed in the selection of rainfall events for the study, and it was found that the flow did not show a significant response mainly due to a lack of surface runoff.

Nevertheless, the current study has not fully explored the surface runoff generation and how it enters the sanitary network and locating the defects in the sewer system for inflow and infiltration has not been discussed yet. They will play an important role in the efficient operation and maintenance management of the pipe network in the future. Therefore, the next step will be to explore how to directly measure inflow and infiltration and determine the degree and location of the defects.

4. CONCLUSION

In the present study, the performance of a sanitary network in a coastal city in China was assessed after a 16-month long-term monitoring. Under dry weather conditions, there is a diurnal flow variation in the study area throughout the observation period. On dry weather days, infiltration was found to be as high as 70% of the total flow under high groundwater levels. On wet weather days, the proportion of RDII was lower than that of GWI for most of the rainfall events in this study, except for typhoon events. It was found that the ratio of the rainfall volume entering the sewer system will reach a limited value when the total rainfall depth increases. This study proposed a reference indicator R_{lim} which is the ratio of rainfall volume entering the sewer system to the total rainfall volume for assessing the conditions of sewer systems in terms of RDII. A higher R_{lim} indicates that the sewer system has a high proportion of water entering the system during storm events, and hence the condition of the system is poor.

Distinguishing the volumes corresponding to RDI and RII from the RDII volume is a limitation of this study. For further work, the accuracy of the RDII flow response can be improved by studying more rainfall events and introducing water quality parameters (e.g. conductivity and COD) based on the material balance equation to solve for the extraneous water quantity. Nevertheless, the results obtained from this work can provide technical support for the construction of diagnostic analysis models for the inflow and infiltration of local intelligent drainage systems and enrich the case studies of the inflow and infiltration of sanitary sewer systems in coastal cities.

ACKNOWLEDGEMENT

The authors appreciate the financial support from the Key R&D Program of Zhejiang Province (2020C03082).

DATA AVAILABILITY STATEMENT

Data cannot be made publicly available; readers should contact the corresponding author for details.

CONFLICT OF INTEREST

The authors declare there is no conflict.

REFERENCES

Bertrand-Krajewski, J.-L., Cardoso, M. A., Ellis, B., Frehmann, T. & Pryl, K. 2006 Towards a better knowledge and management of infiltration and exfiltration in sewer systems: The APUSS project. *Water Practice and Technology* **1** (1), wpt2006021.

Chen, X., Huang, B., Zhang, S., Liu, J., Qian, Y., Wang, C. & Zhu, D. Z. 2022 Performance evaluation of sewer system upgrade in an old residential area in Ningbo, China. *Journal of Environmental Engineering* **148** (8), 04022044.

Cheng, J. C. P. & Wang, M. 2018 Automated detection of sewer pipe defects in closed-circuit television images using deep learning techniques. *Automation in Construction* **95**, 155–171.

Crawford, D., Eckley, P. L. & Pier, E. 1999 Methods for estimating inflow and infiltration into sanitary sewers. *Journal of Water Management Modeling* **7**, R204–17.

De Bénédittis, J. & Bertrand-Krajewski, J.-L. 2005 Infiltration in sewer systems: Comparison of measurement methods. *Water Science and Technology* **52** (3), 219–227.

De Bondt, K., Seveno, F., Petrucci, G., Rodriguez, F., Joannis, C. & Claeys, P. 2018 Potential and limits of stable isotopes (δ18O and δD) to detect parasitic water in sewers of oceanic climate cities. *Journal of Hydrology: Regional Studies* **18**, 119–142.

de Ville, N., Le, H. M., Schmidt, L. & Verbanck, M. A. 2017 Data-mining analysis of in-sewer infiltration patterns: Seasonal characteristics of clear water seepage into Brussels main sewers. *Urban Water Journal* **14** (10), 1090–1096.

Dirckx, G., Van Daele, S. & Hellinck, N. 2016 Groundwater Infiltration Potential (GWIP) as an aid to determining the cause of dilution of waste water. *Journal of Hydrology* **542**, 474–486.

Ellis, J. B. & Bertrand-Krajewski, J.-L. 2010 *Assessing Infiltration and Exfiltration on the Performance of Urban Sewer Systems (APUSS)*. IWA Publishing, London, UK. https://doi.org/10.2166/9781780401652. (accessed 25 May 2023).

Guo, S., Shao, Y., Zhang, T., Zhu, D. Z. & Zhang, Y. 2013 Physical modeling on sand erosion around defective sewer pipes under the influence of groundwater. *Journal of Hydraulic Engineering* **139** (12), 1247–1257.

HACH Official Site. Available from: https://www.hach.com/p-fl900av/FL900AV.97 (accessed 16 June 2023).

Hoes, O. A. C., Schilperoort, R. P. S., Luxemburg, W. M. J., Clemens, F. H. L. R. & van de Giesen, N. C. 2009 Locating illicit connections in storm water sewers using fiber-optic distributed temperature sensing. *Water Research* **43** (20), 5187–5197.

Irvine, K., Rossi, M. C., Vermette, S., Bakert, J. & Kleinfelder, K. 2011 Illicit discharge detection and elimination: Low cost options for source identification and trackdown in stormwater systems. *Urban Water Journal* **8** (6), 379–395.

Jenssen Sola, K., Bjerkholt, J., Lindholm, O. & Ratnaweera, H. 2018 Infiltration and inflow (I/I) to wastewater systems in Norway, Sweden, Denmark, and Finland. *Water* **10** (11), 1696.

Mattsson, J., Mattsson, A., Davidsson, F., Hedström, A., Österlund, H. & Viklander, M. 2016 Normalization of wastewater quality to estimate infiltration/Inflow and mass flows of metals. *Journal of Environmental Engineering* **142** (11), 04016050.

Karpf, C. & Krebs, P. 2011 Quantification of groundwater infiltration and surface water inflows in urban sewer networks based on a multiple model approach. *Water Research* **45** (10), 3129–3136.

Kracht, O. & Gujer, W. 2005 Quantification of infiltration into sewers based on time series of pollutant loads. *Water Science and Technology* **52** (3), 209–218.

Kracht, O., Gresch, M. & Gujer, W. 2007 A stable isotope approach for the quantification of sewer infiltration. *Environmental Science & Technology* **41** (16), 5839–5845.

Kracht, O., Gresch, M. & Gujer, W. 2008 Innovative tracer methods for sewer infiltration monitoring. *Urban Water Journal* **5** (3), 173–185.

Li, T., Zhou, Y.-C. & Li, H. 2008 Quantifying nonstorm-water discharges to storm-Water systems with model analysis. *Journal of Environmental Engineering* **134** (11), 928–932.

Liu, T., Ramirez-Marquez, J. E., Jagupilla, S. C. & Prigiobbe, V. 2021 Combining a statistical model with machine learning to predict groundwater flooding (or infiltration) into sewer networks. *Journal of Hydrology* **603**, 126916.

Ministry of Housing and Urban-Rural Development of the People's Republic of China. 2018 *Standard for Design of Outdoor Water Supply Engineering. GB 50013-2018*. Ministry of Housing and Urban Rural Development of the People's Republic of China, Beijing, China.

National Bureau of Statistics of China. 2022 *High-quality Development of the Construction Industry, Strong Foundation, and Innovative Road to Benefit People's Livelihood – the Fourth in A Series of Reports on Economic and Social Development Achievements Since the 18th National Congress of the Communist Party of China*. Statistics for the National Bureau of Statistics of China, Beijing, China.

Ningbo Meteorological Service Center. Climate profile. Available from: https://www.qx121.com/ (accessed 30 March 2023).

Rezaee, M. & Tabesh, M. 2022 Effects of inflow, infiltration, and exfiltration on water footprint increase of a sewer system: A case study of Tehran. *Sustainable Cities and Society* **79**, 103707.

Shehab, T. & Moselhi, O. 2005 Automated detection and classification of infiltration in sewer pipes. *Journal of Infrastructure Systems* **11** (3), 165–171.

Sowby, R. B. & Jones, D. R. 2022 A practical statistical method to differentiate inflow and infiltration in sanitary sewer systems. *Journal of Environmental Engineering* **148** (1), 06021006.

Staufer, P., Scheidegger, A. & Rieckermann, J. 2012 Assessing the performance of sewer rehabilitation on the reduction of infiltration and inflow. *Water Research* **46** (16), 5185–5196.

Sun, L., Zhu, J., Tan, J., Li, X., Li, R., Deng, H., Zhang, X., Liu, B. & Zhu, X. 2023 Deep learning-assisted automated sewage pipe defect detection for urban water environment management. *Science of The Total Environment* **882**, 163562.

Thapa, J. B., Jung, J. K. & Yovichin, R. D. 2019 A qualitative approach to determine the areas of highest inflow and infiltration in underground infrastructure for urban area. *Advances in Civil Engineering* **2019**, 1–11.

THWater Official Site. Available from: http://www.thuenv.com/ (accessed 16 June 2023).

U.S. Environmental Protection Agency [USEPA]. 2007 *Computer Tools for Sanitary Sewer System Capacity Analysis and Planning*. U.S. Environmental Protection Agency. Available from: https://cfpub.epa.gov/si/si_public_record_report.cfm?dirEntryId=184303 (accessed 10 July 2022).

Weiß, G., Brombach, H. & Haller, B. 2002 Infiltration and inflow in combined sewer systems: Long-term analysis. *Water Science and Technology* **45** (7), 11–19.

Xu, Z., Wang, L., Yin, H., Li, H. & Schwegler, B. R. 2016 Source apportionment of non-storm water entries into storm drains using marker species: Modeling approach and verification. *Ecological Indicators* **61**, 546–557.

Yang, F., Zhang, X., Li, J., Jin, F. & Zhou, B. 2021 Simple method to quantify extraneous water and organic matter degradation in sewer networks. *Environmental Science: Water Research & Technology* **7** (1), 172–183.

Zhang, M., Liu, Y., Dong, Q., Hong, Y., Huang, X., Shi, H. & Yuan, Z. 2017 Estimating rainfall-induced inflow and infiltration in a sanitary sewer system based on water quality modelling: Which parameter to use? *Environmental Science: Water Research & Technology* **4** (3), 385–393.

Zhang, M., Liu, Y., Cheng, X., Zhu, D. Z., Shi, H. & Yuan, Z. 2018 Quantifying rainfall-derived inflow and infiltration in sanitary sewer systems based on conductivity monitoring. *Journal of Hydrology* **558**, 174–183.

Zhao, Z., Yin, H., Xu, Z., Peng, J. & Yu, Z. 2020 Pin-pointing groundwater infiltration into urban sewers using chemical tracer in conjunction with physically based optimization model. *Water Research* **175**, 115689.

Zhou, Q., Situ, Z., Teng, S., Liu, H., Chen, W. & Chen, G. 2022 Automatic sewer defect detection and severity quantification based on pixel-level semantic segmentation. *Tunnelling and Underground Space Technology* **123**, 104403.

First received 16 August 2023; accepted in revised form 16 November 2023. Available online 29 November 2023